Scientific Research Publishing

Advances in Materials Physics and Chemistry, 2022, 12, 323-337
https://www.scirp.org/journal/ampc
ISSN Online: 2162-5328
ISSN Print: 2162-531X

Obtaining and Study Smart Composites in the B_4C-SiC-Si-Al-Al_2O_3—Carbon Fiber System

Zviad Kovziridze, Natela Nijharadze, Gulnazi Tabatadze, Teimuraz Cheishvili, Maia Mshvildadze, Nazibrola Kutsiava, Maia Balakhashvili, Nino Dakhvelidze, Salome Gvazava

Institute of Bionanoceramics and Nanocomposite Technology, Technical University of Georgia, Tbilisi, Georgia
Email: kowsiri@gtu.ge

How to cite this paper: Kovziridze, Z., Nijharadze, N., Tabatadze, G., Cheishvili, Te., Mshvildadze, M., Kutsiava, N., Balakhashvili, M., Dakhvelidze, N. and Gvazava, S. (2022) Obtaining and Study Smart Composites in the B4C-SiC-Si-Al-Al2O3—Carbon Fiber System. *Advances in Materials Physics and Chemistry*, **12**, 323-337.
https://doi.org/10.4236/ampc.2022.1211021

Received: October 20, 2022
Accepted: November 26, 2022
Published: November 29, 2022

Abstract

Goal: To obtain SIALON containing composites by reactive sintering method in SiC-B_4C-Si-Al-Al_2O_3 system. Using this method of synthesis, it became possible to obtain composites with different percentages of SIALON. Our task was also to study the phase composition in the SiC-B_4C-Si-Al-Al_2O_3 system. **Method:** The obtained mass was grounded in an attritor and the consolidated composite was obtained by hot pressing at 1800˚C, 40 minutes, delaying at final temperature for 8 min. under 30 MPa pressure. To study the phase composition of the composites, we conducted an X-ray structural analysis on the DRON-3 device, and to study the microstructure, we conducted research on an optical microscope and a raster electron microscope "Nanolab 7" of the company "OPTON". The values of the electrical parameters of the study composites were calculated on the basis of the obtained "lgp-t" dependence. **Result:** In SiC-B_4C-Si-Al-Al_2O_3 system we obtained composites with a matrix composed of: β-SIALON, silicon carbide, corundum and nanoparticles of boron nitride. **Conclusion:** The phase composition of the obtained composite provides high physical-technical and performance properties of these composites. Compression strength—2187 MPA, Bending strength—285 MPa, Thermal expansion coefficient $a_{20\text{-}700}$-3.8 × 10^{-60} C.

Keywords

Composite, Electron Microscope, Phase Composition, β-SIALON

1. Introduction

SIALON is a general name for a large family of silicon nitride-based ceramic alloys, it was first adopted in the beginning of 1970. β-Sialon is the most well-

known phase. Its chemical formula $Si_{6-Z}Al_ZO_ZN_{8-Z}$ (z = 0 - 4.2) and its hexagonal crystal structure are similar to the structure of β-Si_3N_4.

SIALON is distinguished by: high hardness, strength, wear resistance. It retains these properties under high temperature conditions.

Composites working at high temperatures should be characterized by high density, hardness, thermal resistance and should retain these properties when working at high temperatures. Composites obtained from highly refractory oxide ceramics retain their hardness at high temperatures but are characterized by a high coefficient of thermal expansion and therefore low thermal resistance. Carbide-based ceramics have a relatively high coefficient of thermal expansion, but they are oxidized easily when working at high temperatures. Because of this, science has turned its attention to obtain super high-strength composites—SIALONs [1]-[7]. The results of our work [8] [9] [10] show that the composites obtained with the SIALON matrix are highly refractory materials with high performance properties and retain these properties when working at high temperatures. For the study we used electron microscopic, optical and X-ray phase analysis methods.

The paper describes the preparation of a super-ceramic composite with high macro and micro-mechanical properties of SIALON carbide at relatively low temperatures using an innovative, simple technology. As is known, SIALONS are obtained at temperatures of 1800˚C - 2000˚C. With the help of vitrified (96 mas.% glass phase) perlite—2 - 3 mas.% dopant, we obtained similar material at 1450˚C and in the composition with boron carbide, silicon carbide and aluminum oxide, we were able to obtain eutectic precipitation at relatively low temperature—1620˚C by hot pressing. The material is so hard, that it damaged the diamond beads when trying to treat it, and a 3000 atmosphere water jet failed to cut the specimen.

X-ray is performed on DRON-3. Electron microscopic research was performed on a raster electron microscope "Nanolab 7" of the company "OPTON". No special form of samples is required for this study, only a sample fracture is required. It should be noted that the fracture is better to be new, because after some time the surface of the fracture might be covered with dust particles or oxides, which reduces the contrast and makes it difficult to distinguish phases In addition, the ions continue to move on the surface of the new fracture for some time, which makes the study very interesting.

2. Main Part

To obtain the composites, we prepared mixtures, the composition of which is given in Table 1. To C-10 composite we have added carbon fiber, which is characterized by high elasticity modulus (200 - 935 GPa), high-tensile strength (1 - 3 GPa), with these properties it is the desired component, since it strengthens the composite material [11].

The samples were made in a cylindrical shape by the semi-dry method, the

Table 1. Material composition of CN-9 and CN-10 composites.

Composite index	Composition of the initial component, mass %									
	Prosyanaya kaolin (Ukraine)	Al	Al_2O_3	SiC	Si	Perlite Aragats (Armenia)	Y_2O_3	MgO	B_4C	Carbon fiber
C-9	6.5	18.0	22.0	18.0	22.0	2.0	1.5	1.0	9.0	_
C-10	_	20.0	19.0	20.0	22.0	_	1.5	1.0	13.5	3

molding pressure was 20 MPa. After drying the samples were burned out in a siliteoven at a temperature of 1450˚C, Mode 5˚C/min. At the final temperature the samples were kept for 40 minutes.

The physical-technical characteristics and electrical properties of the finished samples, compression strength and bending strength, impact viscosity, density, thermal resistance and thermal expansion coefficients were studied.

The bending strength was measured on a German-made disrupting machine R-100, which has a device determining the strength limit of the specimens on a three-point bend. The loading speed was 5 mm/hr.

When determining the bending strength limit, the maximum stress is calculated by the following formula:

$$\sigma_{\text{bend.}} = 3/2 \cdot Pl_0 / bh^2$$

where: P is the force at which the sample was disrupted, kg; l_0 distance between supports at 3-point load = 25 mm; b sample cross-section width, mm; h the height on which the stress is applied to the specimen, mm. The test results of C-9 and C-10 composites are given in Table 2.

Impact viscosity was determined by the pendulum impact testing machine. When the sample is crushed, the scale marks the swing angle of the pendulum β. Impact-bending strength is calculated by the following formula:

$$A_{\text{imp.}} = A/S$$

where: A—work spent to crush sample, kilojoules (kJ); S—the cross-sectional area of the samples, m^2. For the C-9 composite samples: the cross-sectional dimensions were 1 cm × 0.35 cm; $a = \frac{6.0}{1 \times 0.35} = 17.14\ \text{kJ/m}^2$; for the C-10 composite samples: the cro1ss-sectional dimensions were 1 cm × 0.2 cm; $a = \frac{6.0}{1 \times 0.2} = 17.50\ \text{kJ/m}^2$.

As can be seen from Table 2, the bending strength and the impact viscosity of both composites (C-9, C-10) are almost the same and amount to 261; 265 MPa and 17.14; 17.50 kj/m^2 respectively. Ceramic composites experience thermal loads and gas-thermal impacts when working at high temperatures. In all ceramic materials there are invisible micro-cracks [12] and when the strength of the product is less than the loads, these loads are converted into the decomposition stress energy. At critical loads, high energies develop, causing decomposition

Table 2. The physical-technical characteristics of C-9 and C-10 composites.

Composite name	Density g/cm^3	Compression strength $\sigma_{press.}$ MPa	Bending strength $\sigma_{bend.}$ MPa	Impact viscosity a, kj/m^2	Thermal resistivity constant, Δa_t (K$^-$)	Thermal expansion coefficient α, 10^{-6} (20˚C - 700˚C)
C-9	3.06	1840.6	261	17.14	-5.7×10^{-3}	3.88
C-10	2.97	2187.5	265	17.50	-2.6×10^{-2}	3.80

of the product.

To determine these energies, Z. Kovziridze proposed a formula for calculating the failure stress energy [13] [14], which establishes a universal interdependence between the failure stress energy of a product, the mass of the product, and the rate of crack development under critical stress conditions. The formula for calculating the failure stress energy is as follows:

$$E_{td} = ma_{c.p.},$$

where E_{td} is the failure stress energy, kilojoules; m-sample mass, g; $a_{c.p.}$—the crack development rate −2000 m/sc.

In our case the sample dimensions were 5.2 × 5.2 × 45 mm, the sample mass was 3.86 g. According to Z. Kovziridze's formula the failure stress energy is:

$$E_{td} = ma_{c.p.} = 3.86 \times 2000 = 7.72 \text{ kJ}.$$

The thermal expansion coefficient of the composites (C-9, C-10) was determined with the help of a quartz vertical dilatometer-DKV for measuring the temperature coefficient of linear thermal expansion in the temperature range (20˚C - 700˚C). **Table 2** and **Figure 1** show that this indicator is the same for both composites and is a = 3.88 and 3.80 × 10^{-6}, respectively.

It is known from the literature [13] that the coefficient of thermal expansion of corundum ceramics is high and is $\alpha_{20\text{-}300C}$= 6.2 × 10^{-6}. While the low-oxygen content of refractory compounds, namely silicon carbide, is a = 5.18 × 10^{-6} and is characterized by high thermal resistance [15] It should be noted that the composites we obtained (C-9, C-10j) are characterized even by a lower coefficient of thermal expansion, respectively a = 3.88 and 3.80 × 10^{-6} and a correspondingly higher thermal resistance, which is very important for composites that have to work for a long time at high temperatures and in an aggressive medium (**Figure 1**).

Electrical characteristics have been established for the composite of both compositions (on the device created by T. Cheishvili—CH-24) which were obtained as a result of the "resistance-temperature" dependence experiment. The volumetric electrical resistance of the composites was determined in the section allowing measurements at high-temperatures in the range of 20˚C - 300˚C, by using an electron ohmmeter as the measuring instrument. Graphite electrodes were placed on the surface of the prismatic samples (the upper measuring electrode had a diameter of 14 mm and the lower measuring electrode had a diameter

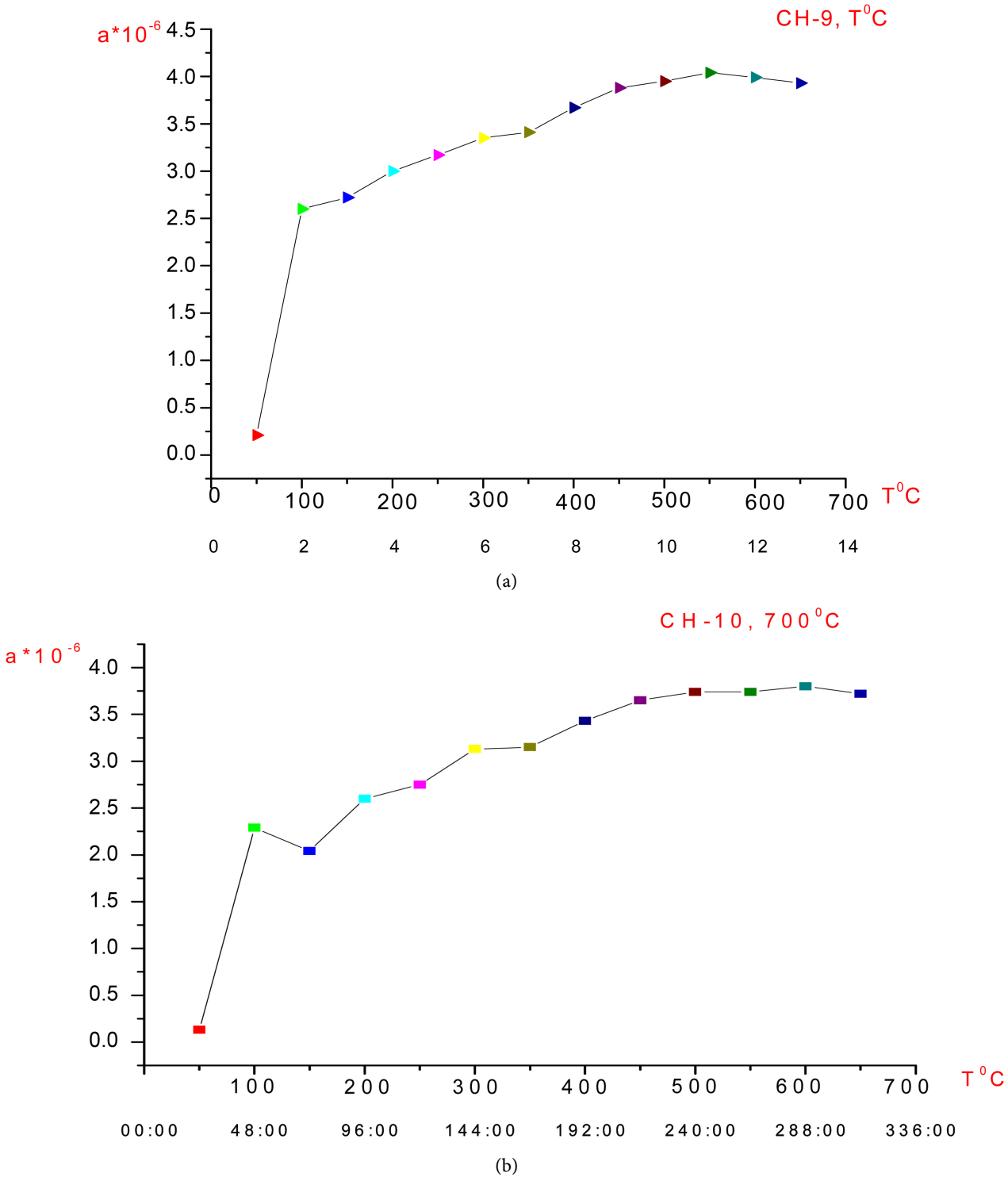

Figure 1. Thermal expansion coefficient and temperature interdependence.

of 16 mm). The dependence of the test specimens on the "specific resistance-temperature" is linear, revealing the peculiarities that an increase in temperature causes a decrease in electrical resistance. Besides the C-9 specimen is characterized by lower values of electric resistance than the specimen C-10. The

difference between the electrical resistances is particularly noticeable at room temperature (the difference is approximately by three degree), but it is less evident at high temperatures (the difference decreases to one degree), which is clear from the material reflecting the results of the experiment (Figure 2).

The values of the electrical parameters of the study composites were calculated on the basis of the obtained "lgp-t" dependence. Three electrical characteristics were determined for both composites: the temperature coefficients of electrical sensitivity (B) and electrical resistivity (α_T) the activation energy of electrical conductivity (E_a), the value of which are presented in Table 3. The difference between the electrical characteristics was found to be significant (C-10 composite data are approximately 5 times higher than those obtained for C-9 composite).

It should be noted that both composites have a negative α_T (resistance decreases with increasing temperature) and low value of E_a (realization of electronic type of electrical conductivity is expected for both materials).

The results obtained should be related to the basic phases represented in C-9 and C-10 composites obtained by the synthesis at 1450˚C, under the same conditions.

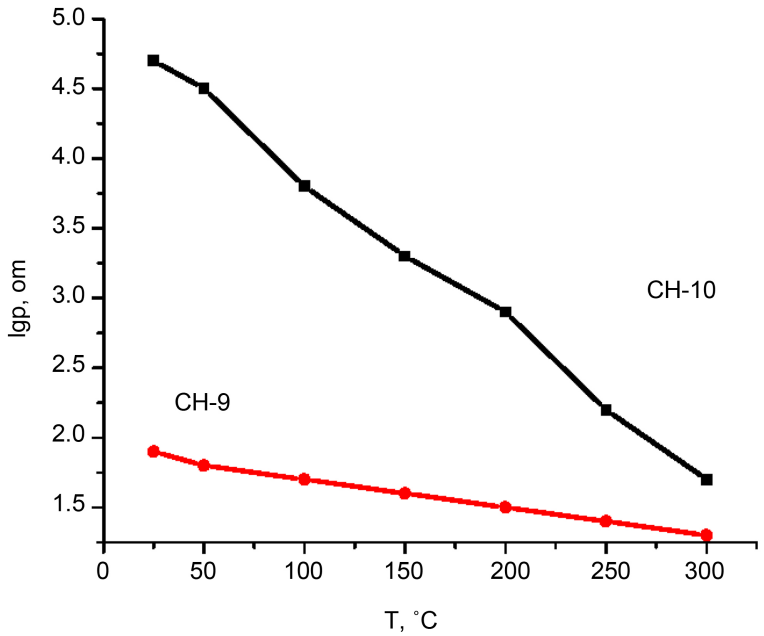

Figure 2. Specific electrical resistance and temperature dependence.

Table 3. Electrical characteristics values of the composites.

Sample №	Coefficient of electrical sensitivity, B (K)	Activation energy of electrical conductivity, ΔE (ev)	Temperature coefficient of electrical resistance, Δa_t (K^-)
C-10	−7170	1.24	-2.6×10^{-2}
C-9	−1560	0.27	-5.7×10^{-3}

According to the results of X-ray phase analysis, the leading phase in the composite of both compositions is SIALON. They also contain five other crystalline compounds of different nature. Due to their electrical properties they can be divided into two groups: Dielectrics (a-Al_2O_3, BN, AlN) and semiconductors (SiC, Si). Considering the identical conditions for obtaining the C-9 and C-10 composites, the factor determining their low resistance and activation energy values could have been the number of SiC and Si solid phases with semiconductor properties existed in the study materials.

Based on the comparison of the electrical characteristics of both composites, it can be assumed that the concentrations of SiC and Si in the C-9 composite must be higher than in the C-10 composite. This could be detected by two approaches: by determining the amount of SiC and Si or by the density of the materials. Both approaches proved to be unusable for C-9 and C-10 composites, since quantitative calculations based on the available X-ray were impossible (due to the abundance of crystal phases and the coincidence of their characteristic intensity peaks) and also the negligible differences between mass densities. (d = 3.02 for C-9; d = 2.98 g/cm^3 for C-10). In any case, the number of SiC in C-9 could not have been higher than in C-10, judging by the material composition of the test composites.

At the same time, X-ray phase analysis revealed the presence of Si in both composites, which could affect the electrical conductivity of the composite. But the Si content in the initial mixture (according to the material compositions) is identical and amounts to wt.22%. At the same time, the C-9 composite body contains two natural rocks (kaolin and perlite) that contain silicon dioxide. Kaolin (6.5 wt.%) and perlite (2.0 wt.%) provide approximately 5.2 wt.% and 3.0 wt.% Si in the C-9 composition, respectively. The reason for this is the structural breakdown of the mineral kaolinite in the geopolymer (kaolin) caused by the temperature and the possibility of conducting the parallelalumothermic process:

$$4Al + 3SiO_2 = 2Al_2O_3 + 3Si\ .$$

This process will result in an additional 2.4% by weight of Si in the C-9 composite, and it is practically expected that the amount of Si in C-9 will be 24.4% by weight. A contributing factor to the uptake of Si from SIO_2 may be the formation of a liquid phase caused by the low-temperature melting of perlite—1240˚C. Aluminum nitride is formed by the reaction of a portion of the aluminum powder in the initial mixture with nitrogen by the following reaction:

$$2Al + N_2 = 2AlN\ .$$

As a result of decomposition of kaolinite at high temperatures part of the aluminum powder restores silicon from SIO_2 according to the reaction above. This process could lead to a change in the ratio between an increase of the amount of semiconductor Si and AlN carrying the insulating properties in favor of Si, this would lead to the increase in electrical conductivity in the C-9 composite.

Structural Study

The test specimens were prepared using the same technology as described in previous papers [16]-[20], *i.e.* the SIALON was synthesized in the nitrogen medium at 1400˚C - 1450˚C, and then the obtained mass was grounded in an attritor and the consolidated composite was obtained by hot pressing at 1800˚C, 40 minutes, delaying at final temperature for 8 min., under 30 MPa pressure.

70 μm of study samples of the composite obtained in this mode were cut from 70 mm diameter and 8 mm thick discs. The cut was made on a 395-M profile grinding machine with a 100 mm-diameter metal binding diamond cutting disc, diamond grain size 50/40 μm, cutter rotation speed 4000 rpm, cutting speed 0.7 mm/min.

The surface of the cut specimens was ground on a 3G71 flat-bottomed grinding machine with a 200 mm-diameter diamond abrasive disc on a Bakelite binder, diamond grainsize-50/40 μm.

Phase analysis of hot-pressed samples was performed on an X-ray machine DRON-3 using CuKα rays.

Examination of the X-ray patterns of the samples burned out at 1400˚C - 1450˚C (**Figure 3**) shows that at 1400˚C the characteristic reflexes of the SIALON are already observed in both composites, and at 1450˚C their intensity is relatively increased. Judging by the intensity of the characteristic peaks of the SIALON, the number of SIALONs formed in the C-9 composite is relatively larger than in the C-10 composite, which can be explained by the presence of kaolin in the C-9 composition. In our opinion, this is due to the nitrogenation of the thermodynamically active kaolinite core $Al_2O_3{\cdot}2SiO_2$, which wasformed as a result of the decomposition of the mineral kaolinite. The following phases have been observed in both composites: Si-AL-O-N, SiC, α-Al_2O_3, BN, and Si (small amount unreacted).

Boron carbide in the composites was converted to boron nitride upon burning out in nitrogen medium at 1400˚C by the following reaction: $B_4C + 2N_2 = 4BN + C$, which in the case of both composites is in small quantities. Newly formed, fine-grained boron nitride improves the microstructure, which is a prerequisite for high mechanical properties, such as: high thermal conductivity, low thermal expansion, good resistance to thermal shocks, easy workability, chemical inertness and low wettability with molten metals. It is used in radiators, boron-alloyed silicon semiconductors, welding trays, crucibles, microwave tubes, sputtering targets, high-precision welding, foundry production, etc.

Analysis performed using an optical microscope showed that the composites in both cases were silicon carbide and corundum grains located in the matrix (**Figure 2**). At the same time the microstructure of C-10 composite is more fine-grained. It can be assumed that during the sintering process of C-9 composite, due to the composition of these composites, more liquid phase is generated than during the sintering process of C-10, contributing to the sintering intensity, which is evidenced by the relatively low porosity of C-9 composite. At the same

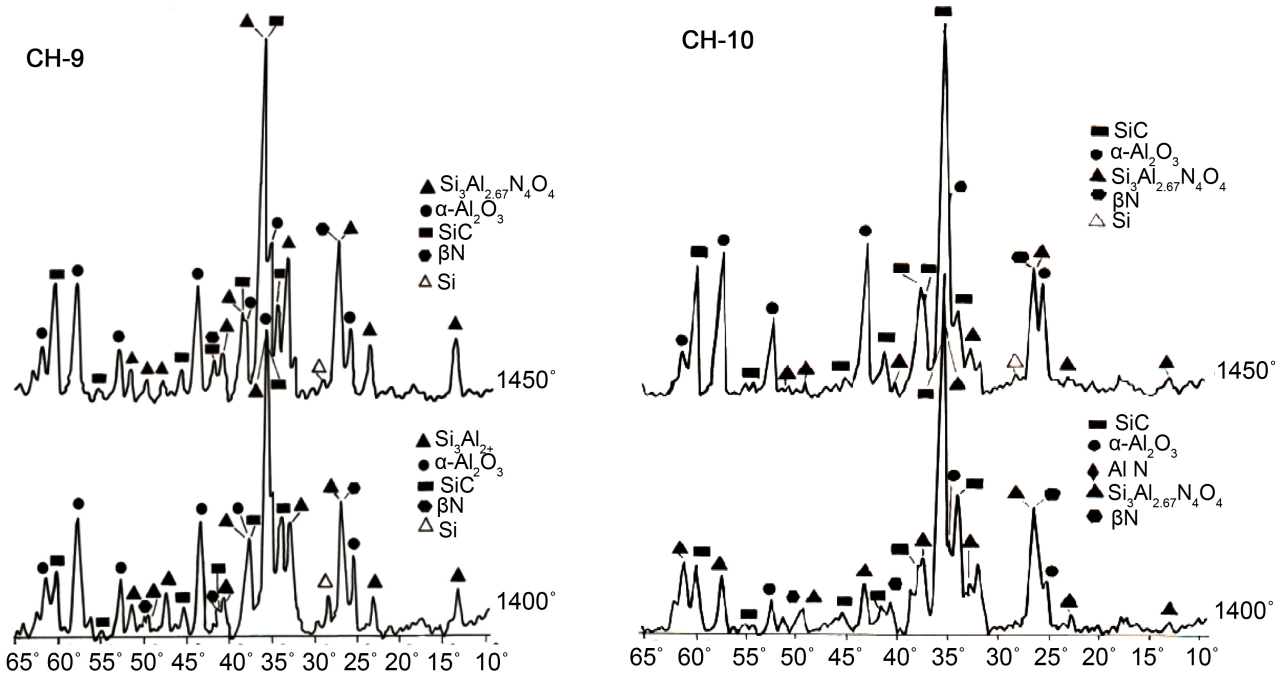

Figure 3. C-9 and C-10 composites X-ray (1400˚C - 1450˚C).

time, the liquid phase promotes the appearance of small grains and their subsequent recrystallization into large grains.

Electron microscopy shows the surface of a well-sintered specimen, on which crystals of the basic phases contained in C-9 composites are clearly seen, namely silicon carbide and corundum grains distributed in the SIALON matrix, even the finest grains of boron nitride are also observed, which are better seen when magnified at close-up (**Figure 4**).

When identifying grains of silicon carbide and corundum, along with SEM images, we relied on the results of X-ray diffraction analysis and X-ray spectral microanalysis.

Figure 5 shows the micro-X-ray spectral analysis images of the C-9 and C-10 composites, the spectrum of the 3 sections and the scheme of the constituent elements, their percentage content, which shows that the main constituent (matrix) of the composite is SiAlON-BN.

The results of micro-X-ray spectroscopy and electron microscopy of the given composites are consistent with X-ray structural analysis. In the matrix of both composites there are represented: β-SiALON-Al_2O_3-SiC, BN crystals are distributed in the matrix (**Figure 6**).

To determine the porosity, we selected the field of vision and determined its area. In the field of vision, we calculated the number of pores according to the size of their diameter; determined the volumetric content and the middle diameter of pores for each composite. The total pore content in C-9 composite is approximately Pvol = 3.7%, for C-10-P_{vol} = 4.8%, the middle size of the pores makes up $P_m \approx 3.75$ and 4.5 μM accordingly.

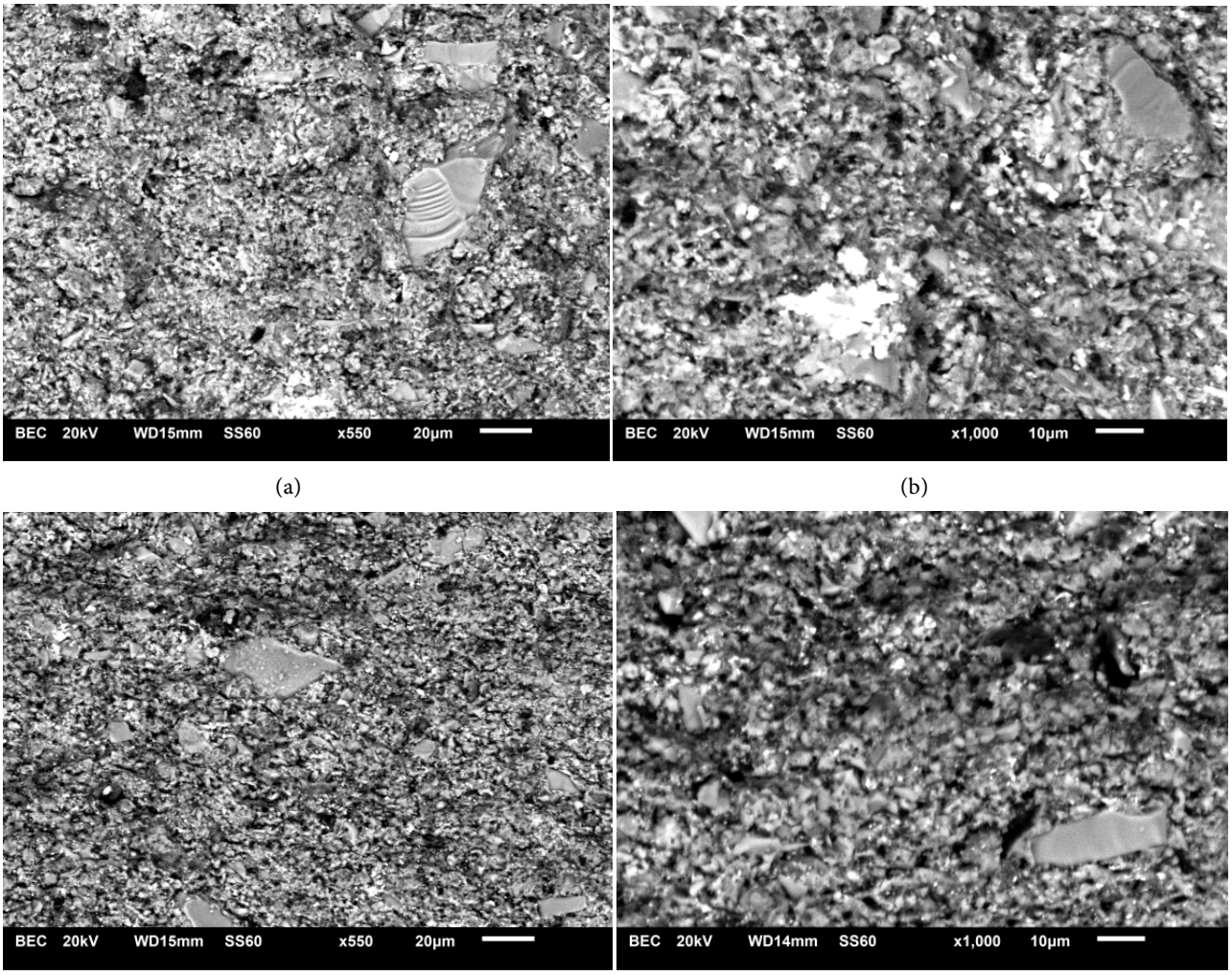

Figure 4. C-9 ((a), (b)) and C-10 ((c), (d)) composites Electronic-microscopic images at different magnifications. X-550; X-1000.

The maximum and minimum size of SiC grains in C-9 composite is 9 - 3 μM, middle size = 6 μM; in C-10 composite is 8 - 4 μM, middle size = 6 μM.

The maximum and minimum size of aluminum oxide grains is 1/1 μM for C-9 composite and 1/0.8 μM for C-10 composite. The average size of aluminum oxide grains in each composite is 1 and 0.8 μM, respectively. As for boron nitride, its dimensions are minimal and approximately equal to an average of 200 nM.

The average grain size in total K_m = 6.5 and 6.6 μM, respectively. Glassy phase volume fraction G_{vol} = 3 and 1% respectively;

Crystal shape factor

$$F_{kf\,\text{C-9}} = D_{\max}/D_{\min} = 10.56/5.54 = 1.91;$$

$$F_{kf\,\text{C-10}} = D_{\max}/D_{\min} = 10.56/6.25 = 1.69.$$

Crystal distribution factor in the matrix by our visual estimation, F_{kd} = 0.9.

The unreacted residue of silicon is about 2 wt.%. In other cases, the Si mass in

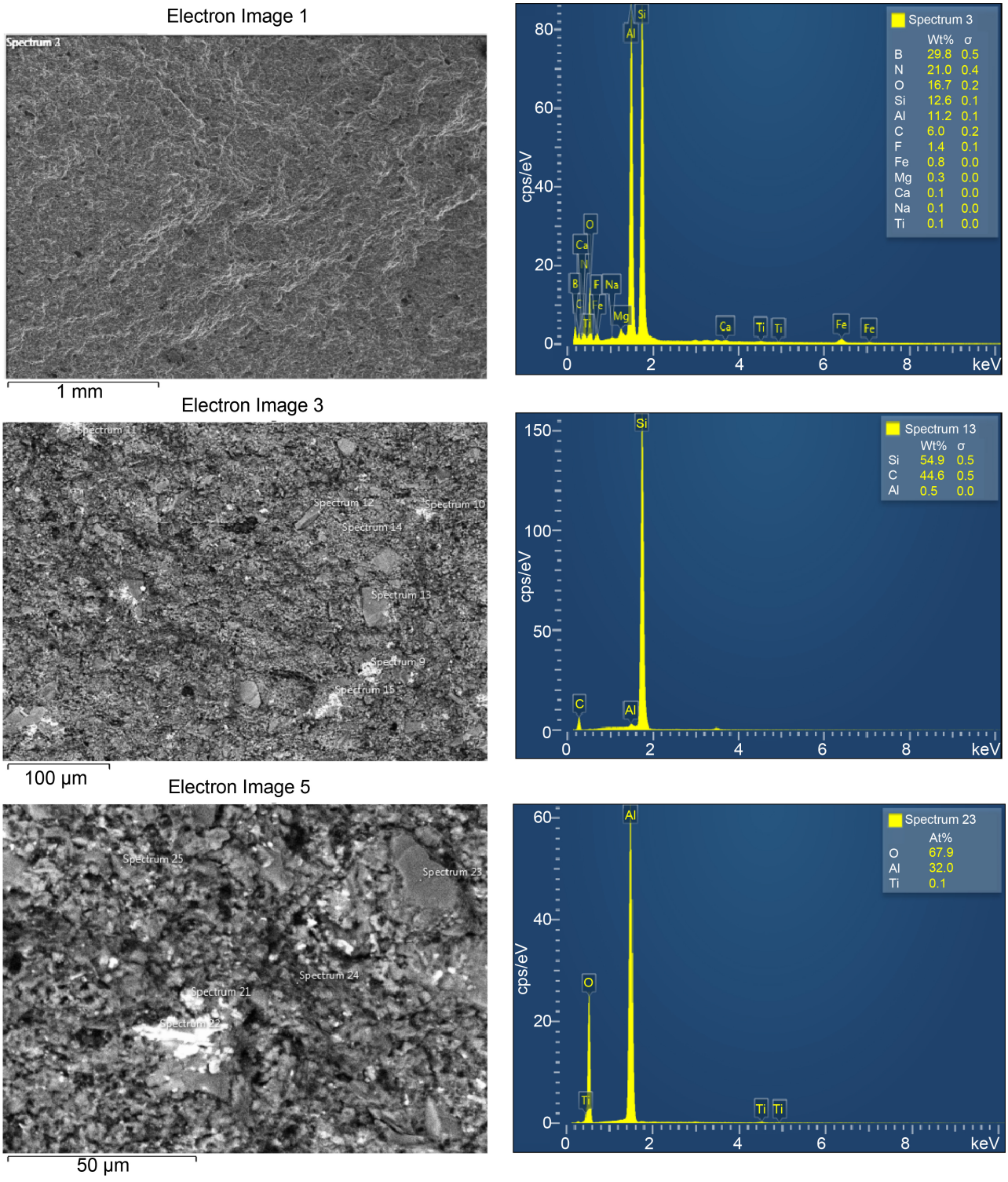

Figure 5. Electronic-microscopic and micro-X-ray spectral images of C-9 composite.

the than initial composition should be taken to be no more 18 - 19 percent. The carbon fiber dopantincreased the mechanical properties by 3 wt.% in C-10 (Table 2). The crystalline phase is: in C-9, 100 − (V porous + V glassy) = 100 − (3.7 + 3) = 93.3, while in C-10: 100 − (V porous + V glassy) = 100 − (4.8 + 1) = 94.2.

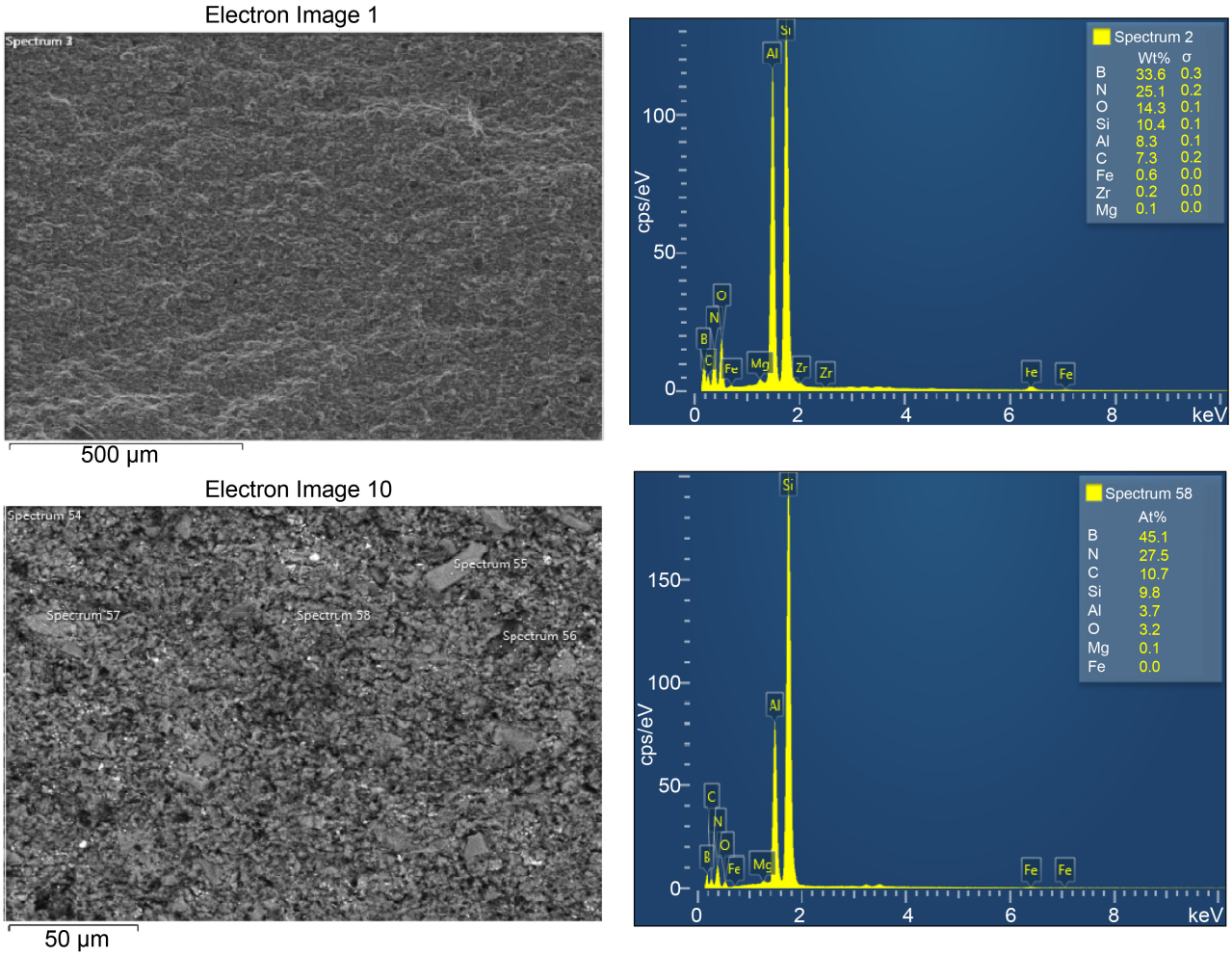

Figure 6. Electronic-microscopic and microrentgeno-X-ray spectral images of C-10 composite.

The dependence of the micro- and macro-mechanical characteristics of the materials on the crystalline phase content in the composite was calculated according to Z. Kovziridze's [21] formula:

$$\sigma_d = \frac{P \cdot F_{kd}}{K_m K_v F_{kf}},$$

where: P load; K_m middle size of crystals; K_v volume fraction of crystals in the matrix; F_{kd} crystals distribution factor in the matrix, which is determined by the researcher; in case of equal distribution it equals to 1, in case of unequal distribution = 0.9; F_{kf} crystal shape factor, is taken as the ratio of the largest characteristic size of a crystal to the smallest, which allows us to characterize the shape of a given set of crystals, according to which we are able to define correlation of mechanical characteristic in the matrix from the crystal phase characteristics in our proposed formula. By inserting the data of Table 4 into the formula we get:

$$\sigma_d = \frac{2187.5 \times 0.9}{6.5 \times 94.2 \times 1.69} = \frac{1968.75}{1035} = 1.9.$$

The dependence of the macro-mechanical characteristics of the materials on

Table 4. Data on phase components in C-9 and C-10 composites.

Composite	Phase name	Field of vision S, μM²	Number of counted grains (pores), n	Grains (pores) Dmid. μM	Max. size of grain (pore) Dmax. μM (average)	Min. size of grain (pore) Dmin. μM (average)	Fκf-shape factor Dmax/Dmin
C-9	SiC	2070	12	11	9	3	
	Al_2O_3		250	1	1	1	
	SiALON		55	14	32	18	
	BN		45	0.2	0.25	0.16	
	Average		90.5	6.5	10.56	5.54	1.91
	Pores		10	3.75	4	3.5	1.15
C-10	SiC	2070	15	10	8	4	
	Al_2O_3		280	0.8	1	0.8	
	SiALON		50	9	33	20	
	BN		45	0.22	0.27	0.18	
	Average		97.5	6.6	10.56	6.25	1.69
	Pores		12	4.5	5	4	1.25

the porous phase content in the composite was also determined according to Kovziridze [22] formula.

$$\sigma_{m/p} = \frac{P}{F_p \cdot P_d \cdot P_{vol} \cdot P_m} = \frac{2187.5}{0.9 \times 1.25 \times 4.5 \times 4.8} = \frac{2187.5}{24.3} = 90 \text{ MPa}/\mu\text{M}^2$$

where: P is load, MPa; F_p shape factor of the pore; P_d pores distribution factor in the matrix. Determination of this value and the evaluation of its significance depend on the researcher, based on the morphological picture depending on how the pores are distributed in the material and what size they are. The value of the factor can vary from 1 to 0.8. If the pores are evenly distributed in the matrix and are about the same size, the factor is determined to be equal to 1; if the pores are unevenly distributed, the factor equals to 0.9 and if the coalescence process of pores is initiated, factor is 0.8; $P_{vol.}$ volumetric fraction of the porous phase in the matrix; P_m the average size of the pores.

3. Conclusion

The obtained composites have been studied and determined the phase composition of the composites; in the case of both composites the main phase, *i.e.* the matrix is SiAlON-SiC-Al_2O_3, in which the BN grains are distributed, originated in the nitrogenation process as a result of the decomposition of boron carbide by nitrogen and the replacement of carbon with nitrogen. The composites are well sintered and the crystals are bonded together with a layer of SiAlON. Material of high physical-technical characteristics is obtained. Composite with low resistance (specific resistance approximately about 10^2 ohm·M), activation energy

(E = 0.27 eV) and the temperature coefficient of electrical resistance ($\Delta\alpha_T$ = 0.057 k^{-1}) with β-SiAlON matrix.

Acknowledgements

We express our gratitude to Shota Rustaveli Georgian National Science Foundation. The work is done with the grant of the Foundation Ys-18-077 Young Scientists Grant 2018.

Conflicts of Interest

The authors declare no conflicts of interest regarding the publication of this paper.

References

[1] Sahin, O., Uzun, O., Sopicka-Lizer, M., Gocmez, H. and Kolemen, U. (2008) Dynamic Hardness and Elastic Modulus Calculation of Porous SiAlON Ceramics Using Depth-Sensing Indentation Technique. *Journal of the European Ceramic Society*, **28**, 1235-1242. https://doi.org/10.1016/j.jeurceramsoc.2007.09.052

[2] Hou, Z., Ye, F. and Liu, L. (2015) Effects of Pore Shape and Porosity on the Dielectric Constant of Porous β-SiAlON Ceramics. *Journal of the European Ceramic Society*, **35**, 4115-4120. https://doi.org/10.1016/j.jeurceramsoc.2015.07.002

[3] Zhang, G.J., Yang, J.F. and Ohji, T. (2001) Fabrication of Porous Ceramics with Unidirectionally Aligned Continuous Pores. *Journal of the American Ceramic Society*, **84**, 1395-1397. https://doi.org/10.1111/j.1151-2916.2001.tb00849.x

[4] Li, B., Liu, K., Zhang, C.R. and Wang, S.Q. (2014) Fabrication and Properties of Borazine Derived Boron Nitride Bonded Porous Silicon Aluminum Oxynitride Wave-Transparent Composite. *Journal of the European Ceramic Society*, **34**, 3591-3595. https://doi.org/10.1016/j.jeurceramsoc.2014.05.041

[5] Yang, J.F., Beppu, Y., Zhang, G.J., Ohji, T. and Kanzaki, S. (2002) Synthesis and Properties of Porous Single-Phase β-SiAlON Ceramics. *Journal of the American Ceramic Society*, **85**, 1879-1881. https://doi.org/10.1111/j.1151-2916.2002.tb00370.x

[6] Zhang, C., Janssen, R. and Claussen, N. (2003) Pressureless Sintering of β-SiAlON with Improved Green Strength by Using Metallic Al Powder. *Materials Letters*, **57**, 3352-3356. https://doi.org/10.1016/S0167-577X(03)00073-9

[7] Hwang, S.-L. and Chen, I.-W. (1994) Reaction Hot Pressing of α- and β-SiAlON Ceramics. *Journal of the American Ceramic Society*, **77**, 165-171. https://doi.org/10.1111/j.1151-2916.1994.tb06972.x

[8] Çalıskan, F. (2014) Improvement in Sinterability of β-SiAlON Produced from Kaolin. *Journal of Alloys and Compounds*, **602**, 140-149. https://doi.org/10.1016/j.jallcom.2014.03.016

[9] Kovziridze, Z., Nijharadze, N., Tabatadze, G., *et al.* (2014) Obtaining of Nanocomposites in SiC-SiAlON and Al_2O_3-SiAlON System by Alumothermal Processes. *Journal of Electronics Cooling and Thermal Control*, **4**, 105-115. https://doi.org/10.4236/jectc.2014.44012

[10] Newcomb, B.A. and Chae, H.G. (2018) Handbook of Properties of Textile and Technical Fibres. Second Edition, Woodhead Publishing, Sawston, 841-871. https://doi.org/10.1016/B978-0-08-101272-7.00021-3

[11] Kovziridze, Z., Nijharadze, N., Tabatadze, G., *et al*. (2016) Smart Materials in the System SiAlON-SiC-Al_2O_3-TiB_2-ZrB_2. *Bit's 2nd Annual World Congress of Smart materials*, Singapore, 4-6 March 2016, 558.

[12] Griffith, A.A. (1920) The Phenomena of Rupture and Flow in Solids. *Philosophical Transactions of the Royal Society of London. Series A*, **221**, 163-198.

[13] Kovzirize, Z. (2018) The Decomposition Stress Energy Formula. *Georgian Ceramics Association, Journal* "*Ceramics and Advanced Technologies*", **1**, 11-23.

[14] Kovziridze, Z. (2018) Failure Stress Energy Formula. *Journal of Electronics Cooling and Thermal Control*, **8**, 31-47. http://www.scirp.org/journal/jectc https://doi.org/10.4236/jectc.2018.83003

[15] Samsonov, G.V. (1978) Physico-Chemical Properties of Oxides. Molkow Metallurgy.

[16] Samsonov, G.V. (1978) Properties of High-Melting-Point Compounds. Short Reference Book. Molkow Metallurgy.

[17] Kovziridze, Z., NiJaradze, N., Tabatadze, G., *et al*. (2014) Obtaining SiAlONs by Nitro-Alum Thermal Processes. *Georgian Ceramics Association, Journal* "*Ceramics and Advanced Technologies*", **2**, 23-31.

[18] Hou, Z., Ye, F. and Liu, L. (2015) Effects of Pore Shape and Porosity on the Dielectric Constant of Porous β-SiAlON Ceramics. *Journal of the European Ceramic Society*, **35**, 4115-4120. https://doi.org/10.1016/j.jeurceramsoc.2015.07.002

[19] Deng, X., Li, X.C., Zhu, B.Q. and Chen, P.G. (2015) *In-Situ* Synthesis Mechanism of Plate-Shaped β-Sialon and Its Effect on Al_2O_3—C Refractory Properties. *Ceramics International*, **41**, 14376-14382.

[20] Yang, J.F., Beppu, Y., Zhang, G.J., Ohji, T. and Kanzaki, S., (2002) Synthesis and Properties of Porous Single-Phase β-SiAlON Ceramics. *Journal of the American Ceramic Society*, **85**, 1879-1881. https://doi.org/10.1111/j.1151-2916.2002.tb00370.x

[21] Kovziridze, Z. (2020) The Formula of Dependence of Mechanical Characteristics of Materials on Crystalline Phase Composition in the Matrix. *Advances in Materials Physics and Chemistry*, **10**, 178-188. https://doi.org/10.4236/ampc.2020.108013

[22] Kovziridze, Z. (2018) Macro-Mechanical Properties Porous Phase Dependence Formula. *Journal of the Georgian Ceramists Association. Ceramics and Advanced Technologies*, **20**, 28-34.